NeuroImage 156 (2017) 109–118

Contents lists available at ScienceDirect

NeuroImage

journal homepage: www.elsevier.com/locate/neuroimage

A novel approach to map induced activation of neuronal networks using chemogenetics and functional neuroimaging in rats: A proof-of-concept study on the mesocorticolimbic system

Theresia J.M. Roelofs[a,b], Jeroen P.H. Verharen[a], Geralda A.F. van Tilborg[b], Linde Boekhoudt[a], Annette van der Toorn[b], Johannes W. de Jong[a], Mieneke C.M. Luijendijk[a], Willem M. Otte[b,c], Roger A.H. Adan[a,1], Rick M. Dijkhuizen[b,*,1]

[a] Department of Translational Neuroscience, Brain Center Rudolf Magnus, University Medical Center Utrecht, Universiteitsweg 100, 3584 CG Utrecht, The Netherlands

[b] Biomedical MR Imaging and Spectroscopy Group, Center for Image Sciences, University Medical Center Utrecht, Bolognalaan 50, 3584 CJ Utrecht, The Netherlands

[c] Department of Pediatric Neurology, Brain Center Rudolf Magnus, University Medical Center Utrecht, Heidelberglaan 100, 3584 CX Utrecht, The Netherlands

ARTICLE INFO

Keywords:
Chemogenetics
DREADD-technology
Functional imaging
Mesocorticolimbic system
Pharmacological fMRI

ABSTRACT

Linking neural circuit activation at whole-brain level to neuronal activity at cellular level remains one of the major challenges in neuroscience research. We set up a novel functional neuroimaging approach to map global effects of locally induced activation of specific midbrain projection neurons using chemogenetics (Designer Receptors Exclusively Activated by Designer Drugs (DREADD)-technology) combined with pharmacological magnetic resonance imaging (phMRI) in the rat mesocorticolimbic system. Chemogenetic activation of DREADD-targeted mesolimbic or mesocortical pathways, i.e. projections from the ventral tegmental area (VTA) to the nucleus accumbens (NAcc) or medial prefrontal cortex (mPFC), respectively, induced significant blood oxygenation level-dependent (BOLD) responses in areas with DREADD expression, but also in remote defined neural circuitry without DREADD expression. The time-course of brain activation corresponded with the behavioral output measure, i.e. locomotor (hyper)activity, in the mesolimbic pathway-targeted group. Chemogenetic activation specifically increased neuronal activity, whereas functional connectivity assessed with resting state functional MRI (rs-fMRI) remained stable. Positive and negative BOLD responses distinctively reflected simultaneous ventral pallidum activation and substantia nigra pars reticulata deactivation, respectively, demonstrating the concept of mesocorticolimbic network activity with concurrent activation of the direct and indirect pathways following stimulation of specific midbrain projection neurons. The presented methodology provides straightforward and widely applicable opportunities to elucidate relationships between local neuronal activity and global network activity in a controllable manner, which will increase our understanding of the functioning and dysfunctioning of large-scale neuronal networks in health and disease.

Introduction

Neuroimaging studies in humans, enabling non-invasive whole-brain mapping of functional networks, have revolutionized the field of cognitive neuroscience. Likewise, neuronal recordings at the cellular level in animal models have provided insights into precise neuronal activity underlying specific behaviors. However, the ability to directly link large-scale neural network activation to micro-scale neuronal circuit activity remains a significant challenge.

Recent developments in chemogenetics and optogenetics have provided unique experimental tools to selectively activate or inhibit targeted neuronal populations or projections in animals (Armbruster et al., 2007; Boyden et al., 2005; Deisseroth, 2015; Urban and Roth, 2015). Chemogenetic stimulation of neurons using Designer Receptors Exclusively Activated by Designer Drugs (DREADD)-technology induces physiologically relevant neuronal activation by increasing neuronal excitability similar to physiological activation via native muscarinic receptors (Urban and Roth, 2015). One of the possible ways to take

* Corresponding author.
E-mail address: r.m.dijkhuizen@umcutrecht.nl (R.M. Dijkhuizen).
[1] Shared senior authorship.

http://dx.doi.org/10.1016/j.neuroimage.2017.05.021
Received 23 January 2017; Accepted 11 May 2017
Available online 11 May 2017

advantage of DREADD-technology is to manipulate specific projection neurons. This can be achieved by intracerebrally delivering floxed activating designer receptors (hM3Dq DREADDs) through adeno-associated viral vectors (AAVs) in the region of origin of the projection, in combination with Cre-recombinase in the projection region through retrograde traveling canine adenoviral vector (CAV2-CRE). The Cre-recombinase enzyme recombines the floxed receptors, leading to their expression on the targeted projection neurons specifically (Boender et al., 2014). The DREADDed projection can subsequently be activated by peripheral injection of the designer ligand clozapine-*N*-oxide (CNO) (Armbruster et al., 2007).

One of the neural systems that has been extensively investigated both in humans and animal models, is the mesocorticolimbic system, which is implicated in many physiological (e.g. reward-related behavior, feeding behavior, decision making, and learning) and pathological (e.g. eating disorders, addiction, and depression) behaviors (Breiter et al., 1997; Malik et al., 2008; Rogers, 2011; Salamone and Correa, 2012; Schultz, 2013; van Zessen et al., 2012; Wang et al., 2012; Wise, 2004). Key pathways of this system include the mesolimbic projection from ventral tegmental area (VTA) to nucleus accumbens (NAcc), and the mesocortical projection from VTA to medial prefrontal cortex (mPFC). Activation of dopamine neurons in the mesolimbic system (involved in reward processing) modulates downstream activity of direct and indirect pathway neurons (Humphries and Prescott, 2010; Kenny et al., 2013; Russo and Nestler, 2013). The strict classical division of the direct and indirect pathways based on medium spiny neurons (MSNs) expressing excitatory dopamine D1- and inhibitory dopamine D2-receptors, respectively, has recently been debated by Kupchik et al. (2015), who showed that mouse ventral pallidum (VP) neurons, originally classified as part of the ventral stream indirect pathway (Richard and Berridge, 2012; Russo and Nestler, 2013), receive inputs from the NAcc via D1- as well as D2-receptor expressing MSNs (Kupchik et al., 2015). It is therefore difficult to predict how these combined excitatory and inhibitory inputs will impact on large-scale mesocorticolimbic network activity. This emphasizes the need for accurate and integrative assessment of neuronal signaling from cellular to network level.

The goal of our study was to develop and apply a method that combines chemogenetics and functional imaging to map whole-brain neural network activity upon activation of a specific neuronal projection. To that aim we employed DREADD-technology to target neurons in the rat brain in a projection-specific manner (Boender et al., 2014). To measure the effect of chemogenetic activation of neuronal pathways on global network activity, we applied blood oxygenation level-dependent (BOLD) functional magnetic resonance imaging (fMRI) in a similar fashion as pharmacological fMRI (phMRI), which allows detection of neural activation induced by brain-targeted drugs (Dijkhuizen and Nicolay, 2003; Honey and Bullmore, 2004; Jenkins, 2012; Leslie and James, 2000). We applied this on the mesocorticolimbic system to elucidate the effect of its activation on global neural network activity.

Methods and materials

Animals

Experiments were approved by the Animal Ethics Committee of the University Medical Center Utrecht, The Netherlands, and were conducted in agreement with Dutch laws ('Wet op de Dierproeven', 1996) and European regulations (Guideline 86/609/EEC).

Healthy male Wistar rats (Crl:WU, Charles River, Sulzfeld, Germany) were housed in pairs under controlled temperature and humidity conditions, with a 12h-light/dark cycle (lights on at 7:00 a.m.). Animals had *ad libitum* access to water and chow, and a perspex tube as cage enrichment. Mean (± standard deviation) body weight before MRI was 480 (± 40) g.

Intracerebral viral vector injection

Rats were divided into five groups to specifically target individual neuronal projections. In three groups DREADD expression was induced in the VTA-NAcc projection (VTA-NAcc group, n=13), the VTA-mPFC projection (VTA-mPFC group, n=11), or the VTA-basolateral amygdala (BLA) projection (VTA-BLA group, n=10) by injecting AAV5-hSyn-DIO-hM3D(Gq)-mCherry into the VTA and CAV2-CRE into projection sites (Fig. 1a). Two additional groups served as control: a Sham group (total: n=8) in which rats received sham vectors either in the VTA-NAcc, the VTA-mPFC or the VTA-BLA projection (AAV5-hSyn-DIO-ChR2-eYFP into the VTA and CAV2-CRE into projection sites), and a Saline group (total: n=11) which had DREADD expression in either the VTA-NAcc, the VTA-mPFC or the VTA-BLA projection and which were treated with saline during MRI, instead of the selective DREADD ligand clozapine-N-oxide (CNO, kindly provided by Bryan Roth, and NIMH Chemical Synthesis and Drug Supply Program) (Armbruster et al., 2007). Viral vector injections were performed as follows: before surgery, rats were anesthetized by an intramuscular injection of a combination of 0.315 mg/kg fentanyl and 10 mg/kg fluanisone (Hypnorm, Janssen Pharmaceutica, Belgium), supplemented with an additional injection when needed. Xylocaine was sprayed on the skull for local anesthesia (Lidocaine 100 mg/ml, AstraZeneca BV, the Netherlands). Using a stereotaxic apparatus (David Kopf), 1 µl of $1.0\times10^{\wedge 9}$ genomic copies/µl of AAV5-hSyn-DIO-hM3D(Gq)-mCherry (UNC Vector Core, USA) was injected bilaterally in the VTA of animals in the experimental groups, as described in Boender et al. (2014) (Fig. 1a). Depending on group assignment, 1 µl of $1.25\times10^{\wedge 9}$ genomic copies/µl of the retrograde vector CAV2-CRE (IGMM, France) was injected bilaterally into the NAcc, the prelimbic part of the mPFC, or the BLA (coordinates relative to Bregma for NAcc: AP+1.20 mm, ML ± 2.80 mm at an angle of 10°, DV-7.50 mm; for mPFC: AP +2.70 mm, ML ± 1.40 mm at an angle of 10°, DV-4.90 mm; for BLA: AP-2.20 mm, ML ± 5.00 mm, DV-9.20 mm). Rats in the Sham group received CAV2-CRE injections similarly as other groups, but received 1 µl AAV5-hSyn-DIO-ChR2-eYFP ($1.0\times10^{\wedge 9}$ genomic copies/µl) bilaterally into the VTA.

MRI experiments started at least two months after viral injections, when virus expression is known to be stabilized.

Home cage locomotor activity

Locomotor activity upon CNO or saline injection was assessed in ten VTA-NAcc and nine VTA-mPFC animals. Rats were temporarily housed individually in 43x43×90-cm PhenoTyper® 9000 home cages (Noldus IT, Wageningen, the Netherlands). PhenoTyper cages were equipped with infrared video cameras to monitor locomotor activity. After habituation, CNO or saline was administered and locomotor activity was tracked from the moment of injection. CNO and saline were given in a counter-balanced design, 24 h apart. Total distance moved was analyzed with EthoVision XT11 (Noldus IT, Wageningen, the Netherlands), using locally weighted scatterplot smoothing.

In vivo MRI

In vivo MRI measurements were conducted using a 9.4T MR system equipped with a 400 mT/m gradient coil (Agilent). A home-built 90 mm diameter Helmholtz volume coil and an inductively coupled 25 mm diameter surface coil were used for signal excitation and reception, respectively. Animals were endotracheally intubated for mechanical ventilation with 1.5% isoflurane in O_2/air (1:4) (ventilation rate: 45–55). A cannula was placed intraperitoneally (i.p.) for injection of CNO or saline. CNO (kindly provided by Bryan Roth, and NIMH Chemical Synthesis and Drug Supply Program) was dissolved in saline (0.9% NaCl) at a concentration of 0.3 mg/ml (Boekhoudt et al., 2017; Boender et al., 2014). End-tidal CO_2 was monitored with a capnograph

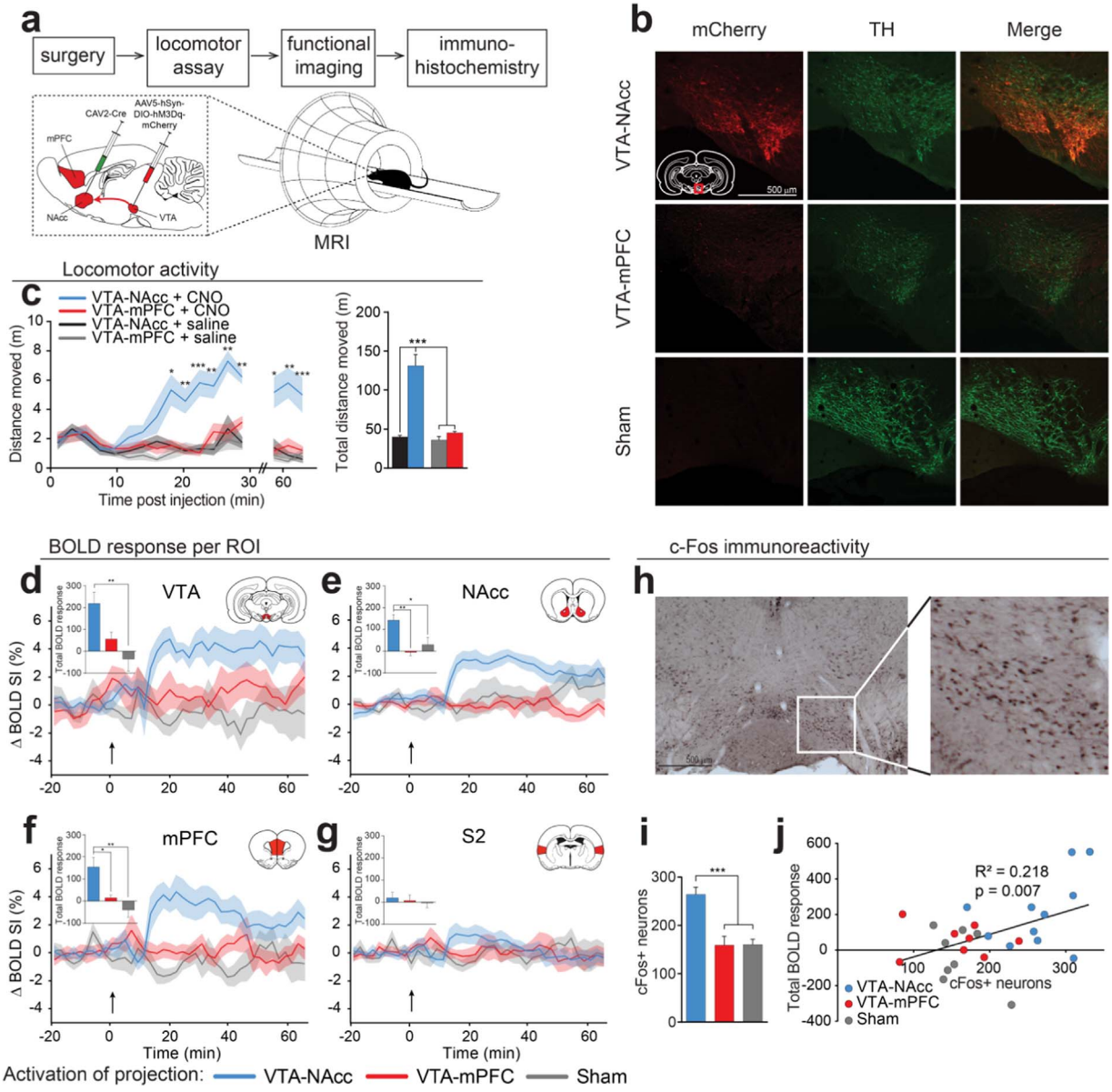

Fig. 1. Novel DREADD-phMRI approach reveals changes in neuronal activity with corresponding time-course as behavioral output and validated by cFos immunohistochemistry. (a) Experimental design. Using a two-vector DREADD approach, only VTA neurons projecting to the NAcc (VTA-NAcc group) or to the mPFC (VTA-mPFC group) express the activating DREADDs. Projection specificity was obtained by injection of AAV5-hSyn-DIO-hM3D(Gq)-mCherry (UNC Vector Core, USA) bilaterally in the VTA, as described in Boender et al. (2014), and the retrograde vector CAV2-CRE (IGMM, France) into the target area. Activation of the targeted pathway in the VTA-NAcc group is schematically represented by the red arrow. (b) Representative images of DREADD expression. DREADD expression is shown in red. TH (tyrosine hydroxylase, a marker for dopamine neurons) was stained in green. DREADD expression was correctly targeted to the VTA. The VTA-NAcc group showed higher expression of DREADDs as compared to the VTA-mPFC group. In the Sham group no DREADDs were expressed. (c) Locomotor activity after CNO or saline injection. A significant interaction effect on total locomotor activity was measured between injection type (CNO or saline), group and time point ($F=3.8$, $p=0.002$). Total distance moved (right graph; mean ± SEM) was significantly different between CNO-injected VTA-NAcc animals (n=10) and other groups ($p < 0.001$, VTA-mPFC group; n=9). Locomotor activity after CNO injection in the VTA-NAcc group started to increase 10 min after injection and was significantly elevated after approximately 20 min which remained up to at least 1 h (*$p < 0.05$, ** $p < 0.01$, *** $p < 0.001$). (d-g) BOLD signal time-courses in the VTA, NAcc, mPFC, and S2, respectively (mean ± SEM) before and after injection of CNO in the VTA-NAcc group, the VTA-mPFC group, and the Sham control group. CNO was injected after 21 min of baseline scanning (arrows). Changes in BOLD signal intensity are presented as percentage change from baseline. The insets show the total BOLD response over the entire phMRI time-course (a.u., mean ± SEM). BOLD signal in the VTA of VTA-NAcc animals started to increase 10 min after injection of CNO and reached a plateau level of 4% higher than baseline after 15–20 min (d). Total BOLD response in the VTA-NAcc (inset) was significantly higher than in the Sham group ($p=0.004$). The VTA in animals from the VTA-mPFC group exhibited a smaller BOLD response, which was not significantly different from the Sham group. Positive BOLD responses in the NAcc (e) and mPFC (f) of the VTA-NAcc group, reached plateau levels of about 3% higher than baseline at 15–20 min after CNO injection, and were significantly elevated as compared to the Sham group ($p=0.018$ for NAcc, and $p=0.003$ for mPFC). Significant responses in the NAcc or mPFC were absent in the VTA-mPFC group. The BOLD signal time-course in the control area S2, not part of the mesocorticolimbic system, remained stable and no significant differences in BOLD signal were found between groups (g). See also Supplementary Fig. S3a for results in the Saline group. (h) Representative image of cFos staining in the VTA of a VTA-NAcc animal, which showed cFos expression after CNO injection. (i) The VTA-NAcc groups expressed significantly more cFos-positive neurons in the VTA as compared to the VTA-mPFC and Sham groups ($p < 0.0005$, mean ± SEM). (j) A positive correlation was found between the number of cFos-positive neurons in the VTA and the total BOLD response in the VTA ($r=0.467$, $p=0.007$). Δ BOLD SI (%): delta BOLD signal intensity in percentages; AAV5: adeno-associated virus serotype 5; CAV2-Cre: canine adenovirus-2 expressing Cre-recombinase; DIO: double-floxed inverted open reading frame; hSyn: human synapsin promotor; mPFC: medial prefrontal cortex; NAcc: nucleus accumbens; S2: secondary somatosensory cortex; VTA: ventral tegmental area. Brain slice insets are adapted from (Paxinos and Watson, 2005).

(Microcap, Oridion Medical 1987 Ltd., Jerusalem, Israel). Body temperature was maintained at 37.0 ± 1.0 °C.

phMRI data were acquired using a gradient echo multi slice (GEMS) sequence, with TR/TE=500/15 ms, flip angle=50°, FOV=32x32×12.5 mm^3, matrix size=128x128×25 voxels, resolution=250x250×500 μm^3, two averages, and a total scan time of 2 min and 8 s per image series. After 10 baseline image series (21.3 min), 1.0 ml/kg CNO or saline was injected i.p. Representative GEMS images are shown in Supplementary Fig. S1.

Next, resting state-fMRI (rs-fMRI) was conducted one hour after CNO injection. For this purpose a 3D gradient echo Echo Planar Imaging (EPI) sequence was used. The read-out and first phase-encode dimensions were covered in a single-shot EPI, the second phase-encode dimension using linear phase encoding. 800 images were acquired with an acquisition time of 730.8 ms per volume (total scan time: 9 min and 45 s), and TR/TE=26.1/15 ms, flip angle=13°, FOV=32.4×32.4×16.8 mm^3, matrix size=54x54×28, and thus an isotropic spatial resolution of 600 µm. Representative EPI images are shown in Supplementary Fig. S2.

Immunohistochemistry

Rats were euthanized by an overdose of isoflurane, followed by intracardial perfusion-fixation as described in Boender et al. (2014). Time between CNO or saline injection and perfusion-fixation was around 90 min to allow synthesis of the peptide product of the immediate early gene cFos. After extraction, brains were post-fixated in 4% paraformaldehyde at 4 °C for at least 24 h and stored in 30% sucrose and 0.1% NaN_3 in PBS. For immunohistochemical assessment of virus expression, 40 µm slices were collected and blocked in 10% normal horse serum (NHS) and 0.25% Triton X-100 in PBS. Subsequently, slices were incubated overnight at 4 °C in primary antibodies rabbit anti-dsRed (1:500, Clontech 632496) and mouse anti-tyrosine hydroxylase (TH, 1:1000, Millipore MAB318) in 2% NHS and 0.1% Triton X-100 in PBS. Rabbit anti-dsRed was directed against mCherry, a red fluorescent tag coupled to the designer receptor. hM3D(Gq)-mCherry was visualized with incubation in secondary antibody Alexa-568- or Alexa-594-labeled goat anti-rabbit (1:500, Abcam ab175471 and A11037), and TH with incubation in Alexa-488-labeled goat anti-mouse (1:1000, Abcam, ab150113), all in 2% NHS and 0.1% Triton X-100 in PBS. Sections were coverslipped with FluorSave (Merck Millipore).

For histochemical quantification of activated neurons at the time of sacrifice, brain sections were stained for cFos. Sections were pre-heated in a 10 mM sodium citrate solution to 80 °C for antigen retrieval, and subsequently incubated in 1% Triton X-100 in PBS, followed by incubation in 0.9% H_2O_2 and 20% methanol in PBS to remove endogenous peroxidase activity. Subsequent blocking in 3% NHS and 0.3% Triton X-100 in PBS, was followed by overnight incubation in primary antibody goat anti-cFos (1:500, Santa Cruz, sc-52-G) in 2% NHS in PBS. Next, slices were incubated in biotinylated secondary antibody horse anti-goat (1:200, Vector, BA-9500) in 1% NHS in PBS, and subsequently in Biotin/Avidin (1:1000, Vectastain) in PBS. This complex was visualized by exposing the slices for exactly 15 min to a solution of liquid DAB (3,3'-Diaminobenzidine, Dako) and 3% nickel ammonium sulphate. All sections were dehydrated using increasing series of ethanol, cleared in xylene, and coverslipped with Entallan (Merck Millipore).

Immunofluorescent sections were photographed by confocal laser scanning microscopy (Olympus Fluoview FV1000). Expression of mCherry on neuronal somas was quantified on an ordinal scale by one of the authors who was blinded for group assignment of the rats. DAB-treated slices stained for cFos were photographed using a Zeiss Axioskop 2 light microscope. In slices comprising the VTA (on average 2–4 per rat), the VTA was manually delineated in ImageJ (Version 1.48 v, National Institutes of Health), and cFos-positive neurons within this area were counted using the cell counter plugin in ImageJ.

Pharmacological fMRI data processing

Pharmacological MR images were corrected for subject motion using *MCFLIRT*; image intensity non-uniformity correction was performed using *n3* (solely for registration purposes); and brain masks were obtained using the *Brain Extraction Tool*, all as implemented in *FSL* (FMRIB's Software Library, http://www.fmrib.ox.ac.uk/fsl, version 5.0.9). Using the affine intermodal image registration tool *FLIRT* (FMRIBs Linear Image Registration Tool) phMRI images were registered to an in-house anatomical MRI template that was matched to a 3D model of a rat brain atlas (Paxinos and Watson, 2005) to create an average phMRI template. PhMRI data were registered to this template, using *FLIRT* followed by *FNIRT* (FMRIBs Nonlinear Image Registration Tool, build 508). PhMRI data were normalized to baseline (average of the ten scans prior to CNO or saline injection). To calculate whole-brain activation maps, phMRI data were smoothed (Gaussian kernel, full width at half maximum = 0.4 mm) and a generalized linear model (GLM)-based analysis was applied to the smoothed phMRI data for each specific group, as described in Mandeville et al. (2014), using the group-specific mean smoothed BOLD signal time-course in the VTA as a regressor. FDR correction for multiple testing was performed and an FDR-corrected Z-value of (-)1.96, corresponding to a p-value of 0.05, was taken as cutoff value for activation maps.

Resting state fMRI data processing

For analyses of rs-fMRI data, images were motion-corrected using *MCFLIRT*, followed by image intensity non-uniformity correction using *n3* (solely for registration purposes). For all animals, rs-fMRI images were registered to images from a single representative rat using *FLIRT* to create an average rs-fMRI data set, which served as a rs-fMRI template. A brain mask of this template was obtained using the *Brain Extraction Tool* in *FSL*. Subsequently the phMRI template, which was matched to an in-house 3D model of a rat brain atlas as described in the data processing section of pharmacological fMRI data, was registered to the rs-fMRI template using *FLIRT*, which allowed consistent ROI analyses of individual rs-fMRI data. Rs-fMRI data were band-pass filtered between 0.01 and 0.1 Hz. Temporal signal to noise ratio (tSNR) was calculated per individual animal using *FSLMATHS* as implemented in *FSL*. The resulting tSNR map was used to mask out voxels with tSNR < 10 and was applied on the 4D filtered rs-fMRI data. Functional connectivity matrices were obtained by calculation of the Fisher-transformed z' of Pearson correlation coefficients *r*.

Data analysis

Locomotor activity over time was analyzed using a mixed factorial ANOVA (repeated measures GLM) analysis, with Greenhouse-Geisser correction for sphericity, in SPSS (v. 16.0). Total locomotor activity per condition was analyzed using a paired-samples t-test and independent-samples *t*-test in SPSS, to compare the effect between treatments and between groups. Four comparisons were made, with Bonferroni correction.

For fMRI analysis, ROIs extracted from the rat brain atlas included the VTA, NAcc, and mPFC. S2, not part of the mesocorticolimbic system, was used as control ROI. BOLD signal time-courses were derived from the phMRI data. Two outlier tests, iterative Grubb's test (GraphPad Software QuickCalcs, http://graphpad.com/quickcalcs/grubbs1/) and iterative Dixon's Q-test (Verma and Quiroz-Ruiz, 2006), were performed on post-injection mean BOLD signal values in the ROIs. The total BOLD response was calculated as area under the curve from the BOLD signal time-course, with mean baseline BOLD signal intensity set to 0. BOLD signal intensity below baseline was interpreted as a negative response, allowing for negative total BOLD response values. Differences in total BOLD response were first compared between the two control groups, to specifically test for any

effect of CNO itself, using an independent samples t-test in SPSS. Next, for all ROIs, total BOLD response values were compared between the CNO-injected groups using one-way ANOVA analysis in SPSS, with Bonferroni correction. Total BOLD response was compared to the number of cFos-positive neurons using a one-tailed Pearson's product-moment correlation test in SPSS. The number of cFos-expressing neurons was compared between the groups using a one-way ANOVA test in SPSS, with Bonferroni correction.

Functional connectivity values calculated from the rs-fMRI experiments were compared between the two control groups using an independent samples t-test in SPSS, to check if CNO by itself had any effect on functional connectivity. Subsequently, functional connectivity values were compared between CNO-injected groups using a one-way ANOVA in SPSS, with Bonferroni correction.

Results

Immunohistochemical assessment of virus expression demonstrated that injections were correctly targeted and resulted in DREADD expression in VTA-NAcc, VTA-mPFC and VTA-BLA projections, representing three different experimental groups. Fig. 1b shows representative examples of DREADD expression in the VTA, which was most abundant in the VTA-NAcc group, in which viral expression was detected on somas in the VTA and on axons in the NAcc core and shell region. No DREADD expression was detected in the rats that received sham vectors (Sham group).

The VTA-BLA group had to be excluded from further analysis, due to low BOLD signal-to-noise ratio in the BLA, caused by air-tissue susceptibility artifacts from the ear cavities. In addition, outlier tests identified two animals from the Saline group with irregular BOLD signal time-courses as outliers, which were excluded from all analyses. Three animals in the VTA-mPFC group showed considerable DREADD expression in the dorsal medial striatum (DMS) and in the medial substantia nigra (SN), indicating that CAV2-Cre virus particles targeted to the mPFC spread to the DMS, and AAV virus particles injected in the VTA spread to the SN. These animals were excluded from further analyses. Final group sizes for phMRI assessment with CNO activation were: VTA-NAcc group: n=13; VTA-mPFC group: n=8; Sham group: n=8. The Saline group in which animals received saline instead of CNO during phMRI consisted of nine animals.

For rs-fMRI analyses, one animal from the VTA-NAcc group, one animal from the VTA-mPFC group, and one animal from the Sham group had to be excluded due to signal distortions.

Locomotor activity

A well-known behavioral output of mesolimbic activation is locomotor (hyper)activity (Boender et al., 2014; Cousins et al., 1993; Ikemoto, 2002; Meredith et al., 2008; Salamone and Correa, 2012). To assess the time course of functional chemogenetic activation, locomotor activity was measured after CNO or saline injections. Total distance moved in the VTA-NAcc group was significantly increased after i.p. injection of CNO as compared to saline (Fig. 1c). Locomotion increased from ten minutes after CNO injection and remained elevated for at least one hour. This confirmed functional chemogenetic activation and indicated the time frame in which injection of CNO results in a behavioral output. In the VTA-mPFC group locomotor activity was unaffected, as expected.

DREADD-induced activation in mesocorticolimbic regions

We applied pharmacological fMRI in animals with projection-specific DREADD expression in the mesolimbic or mesocortical projection (Fig. 1a). During acquisition, animals were under 1.5% isoflurane anesthesia to allow investigation of the effect of chemogenetic activation of defined neuronal projections on global brain activity without interference of conscious processes, differences in arousal state, or stress. Furthermore, the use of anesthetized rats allowed us to compare results to previous optogenetics-fMRI studies which used the same anesthetic (Domingos et al., 2011; Lee et al., 2016, 2010a; Lohani et al., 2016; Voss et al., 2011).

Chemogenetic activation by CNO administration resulted in clear BOLD responses in mesocorticolimbic regions of interest (ROIs) in animals with DREADD expression (Fig. 1d-f). Increased BOLD signal upon injection of CNO remained elevated during the entire phMRI acquisition (i.e., 1 h after CNO injection) (Fig. 1d-f). Significant responses were absent in animals without DREADD expression (Sham group) (Fig. 1d-g), in DREADD-expressing animals that received saline (Saline group) (Supplementary Fig. S3a), and in the control area, the secondary somatosensory cortex (S2), which is not part of the mesocorticolimbic system (Fig. 1g).

Strongest BOLD responses were measured in the VTA-NAcc group. BOLD signal in the VTA started to increase 10 min after injection of CNO and reached a plateau level of 4% higher than baseline after 15–20 min (Fig. 1d). In the NAcc and mPFC, positive BOLD responses reached plateau levels of 3% higher than baseline (Fig. 1e-f). Total BOLD responses in the VTA, NAcc and mPFC of the VTA-NAcc group (insets Fig. 1d-f) were significantly higher than in the Sham group. The VTA in animals from the VTA-mPFC group exhibited a considerably smaller BOLD response (inset Fig. 1d). Significant responses in the NAcc or mPFC regions were absent in the VTA-mPFC group. cFos staining was performed to estimate the number of activated neurons and to correlate this to the phMRI-based measure of neuronal activity. Immunohistochemical analysis showed increased cFos expression in the VTA after CNO injection in animals from the VTA-NAcc group (Fig. 1h), which was significantly higher compared to the Sham and VTA-mPFC groups (Fig. 1i). A significant positive correlation was found between the DREADD-induced BOLD activation response and the number of cFos-positive neurons (Fig. 1j).

DREADD-induced activation of whole-brain networks

To study the causal effects of chemogenetic activation of specific neuronal projections on global brain network activity, we assessed the changes in BOLD signal upon CNO injection at whole-brain level. Fig. 2 shows whole-brain DREADD-induced activation maps of the VTA-NAcc (Fig. 2a) and VTA-mPFC (Fig. 2b) groups, calculated using a generalized linear model (GLM) with the VTA activation response as input signal. Positive and negative BOLD responses were observed throughout the entire brain. Significantly activated or deactivated brain regions are listed in Table 1. In general, the extent of activation was smaller in the VTA-mPFC group as compared to the VTA-NAcc group (Fig. 2 and Table 1).

To check whether DREADD-induced BOLD responses in not directly targeted brain areas were true network effects and not caused by ectopic DREADD expression, we determined the degree of DREADD expression on neuronal somas in primary targeted as well as non-targeted brain regions that showed BOLD responses. No DREADD expression was found in non-targeted regions; one VTA-NAcc animal had considerable expression in the substantia nigra pars reticulata (SNr); and two VTA-NAcc animals had poor expression in the SNr (Supplementary Fig. S4).

Functional connectivity

The effect of chemogenetic activation of mesolimbic and mesocortical pathways on intra- and interhemispheric functional connectivity (fc) was assessed with resting state-fMRI (rs-fMRI) after injection of CNO or saline. Strongest fc was observed between homologous cortical regions, i.e. left and right mPFC, and left and right S2 (Fig. 3 and Supplementary Fig. S3b and S3c). In contrast to our phMRI findings, rs-fMRI did not reveal significant differences in fc of the ROIs between

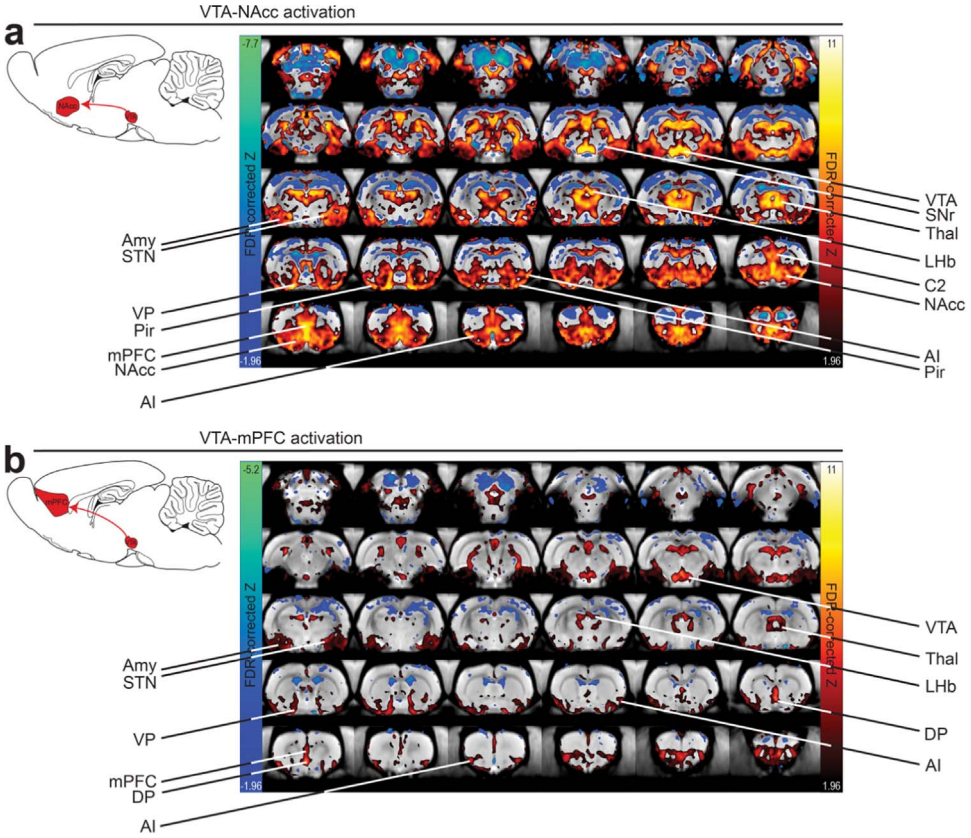

Fig. 2. Detection of network activity in defined neural circuitry in DREADD-targeted animals. The insets on the top left indicate the projection targeted with DREADD-technology. (a) In the VTA-NAcc group, BOLD signal time-course in the NAcc showed strongest correlation to the VTA signal time-course, but correlated responses were also detected in the ventral pallidum (VP), agranular insular cortex (AI), secondary cingulate cortex (C2), amygdaloid nucleus (Amy), piriform cortex (Pir), and thalamic nuclei (Thal). A negative BOLD response was detected in the substantia nigra pars reticulata (SNr). Minor negative signal correlations were detected outside the targeted network. (b) In the VTA-mPFC group, BOLD signal time-course in the mPFC was positively correlated to the VTA signal time-course (mainly infralimbic part and medial prelimbic part). Furthermore, positive signal responses were detected in the VP, AI, Amy, dorsal peduncular cortex (DP), and thalamic nuclei. Also minor negative responses were detected. In both the VTA-NAcc (a) and VTA-mPFC group (b), significant BOLD responses were detected in the subthalamic nucleus (STN) and lateral habenula (LHb). However, caution is needed in interpreting these signals (see Discussion). Insets adapted from (Paxinos and Watson, 2005).

the experimental groups, only interhemispheric fc of the left and right mPFC showed a trend towards being decreased in the VTA-NAcc group as compared to the Sham group (p=0.05).

Discussion

We successfully combined DREADD-technology and pharmacological fMRI to map whole-brain network activity caused by activation of specific midbrain neurons in rats. We detected robust positive BOLD signal responses in DREADD-targeted brain regions, as well as positive and negative BOLD responses in remotely connected direct and indirect pathways of the mesocorticolimbic network. The measured time-course of activation of the VTA-NAcc projection matched with the time-course of increased locomotor activity, a behavioral output of mesolimbic dopamine stimulation. Neuronal activation of the VTA was histologically confirmed by increased cFos expression, although there was quite some variation associated with background expression of cFos. Chemogenetic activation specifically affected neuronal activity, as functional connectivity between mesocorticolimbic regions, as assessed by resting state-fMRI, was not significantly altered by DREADD activation.

Activation of directly targeted projection areas

DREADD-induced activation of VTA neurons projecting to the NAcc caused a significant positive BOLD signal response in the VTA and NAcc, starting 10 min after injection of CNO, in correspondence with the timing of locomotor hyperactivity. In contrast, animals in the VTA-mPFC group exhibited only a weak BOLD signal response in the VTA and mPFC. Likewise, the extent of activation on the whole-brain map of this group was smaller. These findings are likely explained by the lower number of neurons in the VTA-mPFC projection as compared to the VTA-NAcc projection. This was confirmed with immunohistochemistry, showing less DREADD expression in the VTA of VTA-mPFC animals as compared to VTA-NAcc animals. It is unlikely that issues with the CAV or AAV vectors caused low DREADD expression, since the same vectors were used in the VTA-NAcc and Saline groups, which showed high DREADD expression. Although the activation response in the mPFC of VTA-mPFC animals failed to reach statistical significance in the ROI analysis, encompassing the entire mPFC, significant subregional activation was detectable on the statistical activation maps at single voxel level.

Activation and deactivation of connected network regions

phMRI data from the VTA-NAcc group demonstrated that downstream connected brain regions were also activated. Surprisingly, VTA-mPFC activation resulted in an activation pattern that largely overlapped with the activation pattern upon VTA-NAcc stimulation. However, the NAcc was not activated in the VTA-mPFC group, which suggests that projections originating from mPFC neurons (that receive input from the VTA) activate the mesocorticolimbic system independent of accumbens activity. Future studies that allow detailed assessment of the connections of neurons within this network, for example using confocal microscopy of brain slices or light

Table 1
Brain regions exhibiting significant positive (activated) or negative (deactivated) BOLD responses after CNO injection in rats with projection specific DREADD expression.

DREADD-targeted projection	Activated regions	Z-score	Activated part of ROI (%)	Deactivated regions	Z-score	Deactivated part of ROI (%)
VTA-NAcc	VTA	7.0	71	SNr	−3.4	34
	NAcc	6.6	99	IC	−5.0	90
	mPFC	5.9	87	Cerebellar regions	–	–
	VP	4.5	94	Dorsal cortical areas outside targeted network	–	–
	AI	5.2	88			
	C2	4.7	84			
	Amy	5.0	80			
	Pir	5.1	87			
	Thalamic nuclei (mainly: IAM, AM, VA, IMD, MDT, CL, PC)	6.0	83			
	STN[a]	4.7	81			
	LHb[a]	5.2	75			
VTA-mPFC	VTA	4.4	64	IC	−2.8	77
	mPFC (predominantly IL and medial PL)	3.2	33	Dorsal cortical areas outside targeted network	–	–
	VP	3.1	39			
	AI	3.5	50			
	Amy	3.2	60			
	DP	3.1	25			
	Thalamic nuclei (mainly: IAM, AM, IMD, MDT, CL, PC)	3.2	29			
	STN[a]	2.7	42			
	LHb[a]	2.7	25			

Z-scores are calculated as mean FDR-corrected Z-score across significantly (de)activated voxels within regions of interest. A Z-score of (-)1.96 corresponds to a p-value of 0.05. Z-scores in thalamus are calculated within the sub regions mentioned in the left column.

[a] Activity in these regions should be interpreted with caution, because of possible partial volume effects. AI, agranular insular cortex; AM, anteromedial thalamic nucleus; Amy, amygdaloid nucleus; C2, secondary cingulate cortex; CL, centrolateral thalamic nucleus; DP, dorsal peduncular cortex; IAM, interanteromedial thalamic nucleus; IC, inferior colliculae; IL, infralimbic region of medial prefrontal cortex; IMD, intermediodorsal thalamic nucleus; LHb, lateral habenula; MDT, mediodorsal thalamic nucleus; mPFC, medial prefrontal cortex; NAcc, nucleus accumbens; PC, paracentral thalamic nucleus; Pir, piriform cortex; PL, prelimbic region of medial prefrontal cortex; SNr, substantia nigra pars reticulata; STN, subthalamic nucleus; VA, ventral anterior thalamic nucleus; VP, ventral pallidum; VTA, ventral tegmental area.

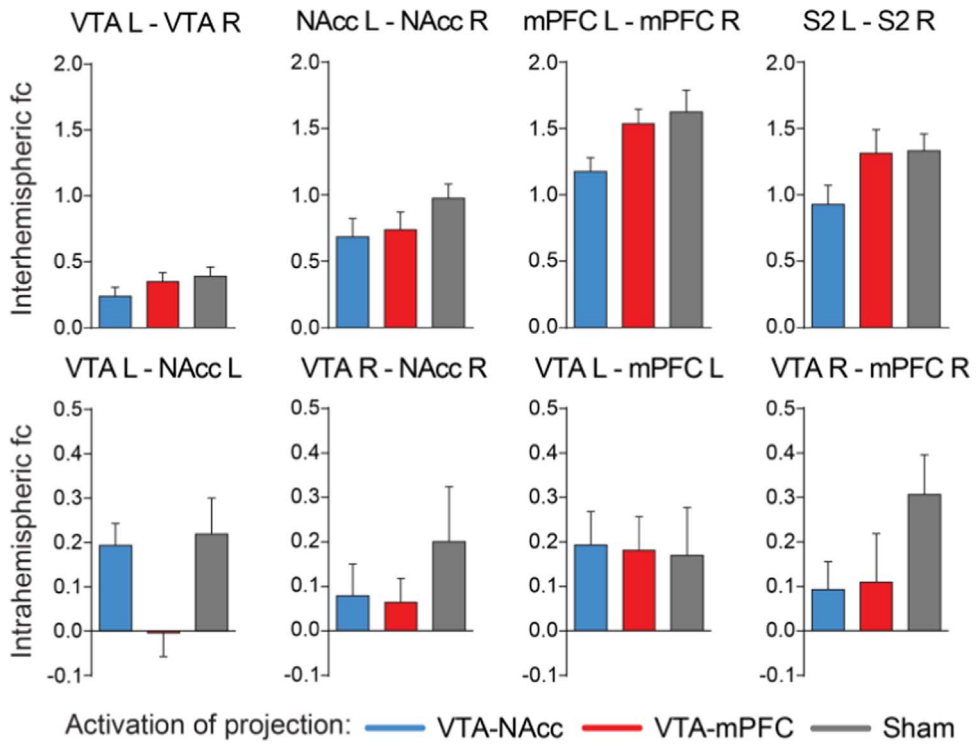

Fig. 3. Unaffected inter- and intrahemispheric functional connectivity. Interhemispheric functional connectivity (fc; mean ± SEM) between bilateral ROIs (upper graphs), and intrahemispheric fc (mean ± SEM) between the left/right VTA and the left/right NAcc or mPFC. Fc is expressed as the Fisher-transformed correlation coefficient (z'). No statistically significant differences in inter- nor in intrahemispheric fc were found between any of the groups. Only intrahemispheric fc between the left and right mPFC showed a trend of reduction in the VTA-NAcc group (p=0.05). See also Supplementary Fig. S3b and S3c for functional connectivity in the Saline group. fc: functional connectivity; mPFC: medial prefrontal cortex; NAcc: nucleus accumbens; S2: secondary somatosensory cortex; VTA: ventral tegmental area.

sheet microscopy of cleared whole-brain tissue, may provide improved insights in the structural organization of these networks.

We have found that on average 80% of DREADD-expressing NAcc-projecting VTA neurons and 72% of mPFC-projecting VTA neurons are TH-positive, thus dopaminergic (unpublished data). Activity in the VTA-NAcc projection induces release of dopamine in the NAcc, which binds to excitatory dopamine D1 receptors and inhibitory dopamine D2 receptors on local MSNs (Humphries and Prescott, 2010; Kenny et al., 2013; Russo and Nestler, 2013). Consequent excitation or inhibition via the direct or indirect pathways explains the observed positive or negative BOLD responses in connected network regions, as outlined below.

The observed negative BOLD responses in the SNr concur with activation of D1-dominant direct pathway MSNs, which project directly to the SNr with GABAergic control (Humphries and Prescott, 2010; Kenny et al., 2013; Russo and Nestler, 2013). Three out of thirteen animals in the VTA-NAcc group expressed some DREADDs in the medial part of the SNr, probably due to minor leakage from the VTA injection site. Circuit-wise, the SNr, which is inhibited by GABAergic control from D1-dominant MSNs and which is also GABAergic itself, subsequently disinhibits the thalamus. The thalamus indeed displayed strong activation in the VTA-NAcc and VTA-mPFC groups. Activation of the indirect pathway would result in net inhibition of the thalamus via an extra inhibitory loop from D2-expressing GABAergic MSNs projecting to VP/globus pallidus externus, which also inhibits the SNr (Humphries and Prescott, 2010; Kenny et al., 2013; Russo and Nestler, 2013). The release of dopamine upon mesocorticolimbic activation binds inhibitory D2 receptors on indirect pathway MSNs, leading to inhibition of the indirect pathway. The observed activation of the VP after stimulation of the VTA-NAcc projection presumably results from disinhibition via the D2-dominant GABAergic projection from NAcc MSNs to the VP (Humphries and Prescott, 2010; Kenny et al., 2013; Russo and Nestler, 2013). Although it was recently described that the VP does not only receive input from the NAcc via D2-, but also via D1-expressing MSNs (Kupchik et al., 2015), our study shows that the net effect of VTA-NAcc activation is an activation of the VP, likely resulting from disinhibition via D2 GABAergic MSNs. At the level of the thalamus, the direct and indirect pathways converge. Direct pathway activation combined with indirect pathway inhibition synergistically activates the thalamus and cortical output areas of the mesocorticolimbic system, as was observed in our data.

The mediodorsal nucleus of the thalamus (MDT), which showed a positive activation response in the VTA-NAcc and VTA-mPFC groups but no DREADD expression, activates the cingulate, infralimbic, prelimbic and agranular insular cortices, forming a striato-pallido-thalamo-cortical circuit (Groenewegen, 1988; Groenewegen et al., 1993; Ikemoto, 2007). These forebrain circuits involving basal ganglia, thalamus and (pre)frontal cortical areas, run via the direct as well as the indirect pathway. This entire neural circuit, commonly known as the direct and indirect striatal output pathways, exhibited significant BOLD responses. The subthalamic nucleus (STN) and lateral habenula (LHb), forming an integrated part of this circuit, were both significantly activated upon VTA-NAcc as well as VTA-mPFC stimulation. However, phMRI signals in the STN and LHb should be interpreted with caution, because of their small size and close proximity to larger areas with strong responses.

The detection of simultaneous direct and indirect pathway activity demonstrates the ability of DREADD-phMRI to gauge network activity upon activation of specific neuronal pathways. Previously, fMRI has been successfully employed to map and measure optogenetically-induced changes in BOLD fMRI signals (Decot et al., 2016; Desai et al., 2011; Domingos et al., 2011; Ferenczi et al., 2016; Lee et al., 2016, 2010b; Lohani et al., 2016; Voss et al., 2011). In contrast to our study, some optogenetics-fMRI papers in which the VTA was targeted in TH::Cre animals reported clear activation of the dorsal striatum (Decot et al., 2016; Ferenczi et al., 2016; Lohani et al., 2016). Since the medial SN is located adjacent to the lateral VTA and projects to the DMS (Boekhoudt et al., 2016), we believe that unintended targeting of the medial SN together with the VTA may have resulted in activation of the dorsal part of the striatum. By using a Cav2-Cre approach, we exclusively targeted VTA neurons projecting to the NAcc (in the VTA-NAcc group) and prevented coactivation of VTA-DMS neurons.

Our study revealed BOLD responses which were considerably stronger compared to earlier studies employing optogenetics-fMRI in the same neural networks (Ferenczi et al., 2016; Lee et al., 2016; Lohani et al., 2016; Voss et al., 2011). Chemogenetics offers a valuable alternative, since it bypasses potential optogenetics-related artifacts in BOLD signal caused by optic probe implantation, laser-induced tissue heating and unspecific light-induced activation of visual pathways (Christie et al., 2013; Schmid et al., 2016). Chemogenetics is easily applied, allows for selective activation of specific neuronal cell-types and projections, and can be straightforwardly combined with fMRI (Gozzi et al., 2010; Baslow et al., 2016). A disadvantage of chemogenetically induced activation, however, is the lack of control of the activation duration, for example due to incomplete understanding of CNO's pharmacokinetic properties.

Recently, Lee et al. showed that activation of direct and indirect pathway MSNs results in opposing brain-wide responses (Lee et al., 2016). They specifically targeted D1 or D2 receptor-expressing neurons using optogenetics and, with fMRI, confirmed the long-standing hypothesis that the direct and indirect pathways exert antagonistic control over neural networks. Our results nicely match the results described by Lee and colleagues, and corroborate the potential of phMRI to detect these defined pathways. The robust BOLD signal responses detected in our study illustrate the suitability and potential of DREADD-technology when combined with functional neuroimaging.

Stable functional connectivity

Despite the clear detection of chemogenetically induced BOLD responses with phMRI, rs-fMRI revealed no significant changes in inter- and intrahemispheric functional connectivity between mesocorticolimbic ROIs. This result suggests that chemogenetic activation of specific pathways only affects activity of the targeted areas and leaves functional connectivity unaffected. Although this may appear as a discrepancy, the underpinnings of brain activation and functional connectivity are conceptually different. Brain activation reflects an external stimulus-induced increase in neuronal activity (measured by model-fitting for phMRI), whereas functional connectivity reflects intrinsic spontaneous neuronal signal synchronization (measured from interregional temporal correlation for rs-fMRI). Although functional connectivity is a determining factor for network activation, it does not consequentially change when networks are activated.

Our findings of an absent apparent effect of neuronal activation on functional connectivity seem in contrast with results from Ferenczi et al. (2016) who reported that an optogenetically induced increase in excitability of mPFC neurons led to significant modulation of resting state networks. Differences in stimulation paradigm, neuronal signaling and awake vs. anesthetized may explain the dissimilar effects on functional connectivity. Ferenczi et al. stimulated predominantly excitatory glutamatergic pyramidal neurons in the mPFC using optogenetics in awake rats and used a different rs-fMRI protocol. They induced neuronal activation directly before the rs-fMRI acquisition, whereas our rs-fMRI data were acquired 1 h after CNO injection. This may have weakened a possible effect on functional connectivity in our study. However, our phMRI data and previous behavioral data (Boekhoudt et al., 2017) indicate that DREADD-induced neuronal activation persists for more than an hour. Although fMRI in awake rats may allow for better translation to human fMRI data, the use of anesthetized animals enabled us to specifically study the causal effects of chemogenetically induced activation, without interference of conscious processing, arousal state, stress or pain.

Conclusions

Our proof-of-principle study demonstrates that DREADD-phMRI offers a potent new tool to assess large-scale network activity – at whole-brain level – in response to activation of specific neuronal pathways – at cellular level. We showed that activation of mesocorticolimbic projection neurons triggered network activity patterns that provided new insights in the involvement of the direct and indirect pathways. Because of the relative ease of use and physiological nature of the induced neuronal activation, we envision a broad range of applications for DREADD-phMRI. The potential to modulate and monitor activity of neuronal circuits with DREADD-phMRI provides a novel tool to bridge the gap between fundamental neuroscience and (human) neuroimaging studies, giving better insights in the functioning and dysfunctioning of neural networks.

Acknowledgments

This work was supported by the European Union Seventh Framework Program (FP/2007–2013) [grand number 607310 (Nudge-it)], and by the Netherlands Organization for Scientific Research [NWO-VICI 016.130.662]. The funding sources had no involvement in the collection, analysis, or interpretation of the data, nor in the writing or submission of this article. We thank Caroline van Heijningen for assistance on immunohistochemistry and Gerard van Vliet for technical assistance.

Appendix A. Supplementary material

Supplementary data associated with this article can be found in the online version at doi:10.1016/j.neuroimage.2017.05.021.

References

Armbruster, B.N., Li, X., Pausch, M.H., Herlitze, S., Roth, B.L., 2007. Evolving the lock to fit the key to create a family of G protein-coupled receptors potently activated by an inert ligand. Proc. Natl. Acad. Sci. USA 104, 5163–5168. http://dx.doi.org/10.1073/pnas.0700293104.

Baslow, M.H., Cain, C.K., Sears, R., Wilson, D.A., Bachman, A., Gerum, S., Guilfoyle, D.N., 2016. Stimulation-induced transient changes in neuronal activity, blood flow and N-acetylaspartate content in rat prefrontal cortex: a chemogenetic fMRS-BOLD study. NMR Biomed. 29, 1678–1687. http://dx.doi.org/10.1002/nbm.3629.

Boekhoudt, L., Omrani, A., Luijendijk, M.C.M., Wolterink-Donselaar, I.G., Wijbrans, E.C., van der Plasse, G., Adan, R.A.H., 2016. Chemogenetic activation of dopamine neurons in the ventral tegmental area, but not substantia nigra, induces hyperactivity in rats. Eur. Neuropsychopharmacol. 26, 1784–1793. http://dx.doi.org/10.1016/j.euroneuro.2016.09.003.

Boekhoudt, L., Roelofs, T.J.M., de Jong, J.W., de Leeuw, A.E., Luijendijk, M.C.M., Wolterink-Donselaar, I.G., van der Plasse, G., Adan, R.A.H., 2017. Does activation of midbrain dopamine neurons promote or reduce feeding? Int. J. Obes., 1–34. http://dx.doi.org/10.1038/ijo.2017.74.

Boender, A.J., de Jong, J.W., Boekhoudt, L., Luijendijk, M.C.M., van der Plasse, G., Adan, R.A.H., 2014. Combined use of the canine adenovirus-2 and DREADD-technology to activate specific neural pathways in vivo. PLoS One 9, e95392. http://dx.doi.org/10.1371/journal.pone.0095392.

Boyden, E.S., Zhang, F., Bamberg, E., Nagel, G., Deisseroth, K., 2005. Millisecond-timescale, genetically targeted optical control of neural activity. Nat. Neurosci. 8, 1263–1268. http://dx.doi.org/10.1038/nn1525.

Breiter, H.C., Gollub, R.L., Weisskoff, R.M., Kennedy, D.N., Makris, N., Berke, J.D., Goodman, J.M., Kantor, H.L., Gastfriend, D.R., Riorden, J.P., Mathew, R.T., Rosen, B.R., Hyman, S.E., 1997. Acute effects of cocaine on human brain activity and emotion. Neuron 19, 591–611.

Christie, I.N., Wells, J.A., Southern, P., Marina, N., Kasparov, S., Gourine, A.V., Lythgoe, M.F., 2013. fMRI response to blue light delivery in the naïve brain: implications for combined optogenetic fMRI studies. Neuroimage 66, 634–641. http://dx.doi.org/10.1016/j.neuroimage.2012.10.074.

Cousins, M.S., Sokolowski, J.D., Salamone, J.D., 1993. Different effects of nucleus accumbens and ventrolateral striatal dopamine depletions on instrumental response selection in the rat. Pharmacol. Biochem. Behav. 46, 943–951. http://dx.doi.org/10.1016/0091-3057(93)90226-J.

Decot, H.K., Namboodiri, V.M., Gao, W., McHenry, J.A., Jennings, J.H., Lee, S.-H., Kantak, P.A., Kao, Y.-C., Das, M., Witten, I.B., Deisseroth, K., Shih, Y.-Y., Stuber, G.D., 2016. Coordination of brain wide activity dynamics by dopaminergic neurons. Neuropsychopharmacology 42, 1–32. http://dx.doi.org/10.1038/npp.2016.151.

Deisseroth, K., 2015. Optogenetics: 10 years of microbial opsins in neuroscience. Nat. Neurosci. 18, 1213–1225.

Desai, M., Kahn, I., Knoblich, U., Bernstein, J., Atallah, H., Yang, A., Kopell, N., Buckner, R.L., Graybiel, A.M., Moore, C.I., Boyden, E.S., 2011. Mapping brain networks in awake mice using combined optical neural control and fMRI. J. Neurophysiol. 105, 1393–1405. http://dx.doi.org/10.1152/jn.00828.2010.

Dijkhuizen, R.M., Nicolay, K., 2003. Magnetic resonance imaging in experimental models of brain disorders. J. Cereb. Blood Flow Metab. 23, 1383–1402. http://dx.doi.org/10.1097/01.WCB.0000100341.78607.EB.

Domingos, A.I., Vaynshteyn, J., Voss, H.U., Ren, X., Gradinaru, V., Zang, F., Deisseroth, K., de Araujo, I.E., Friedman, J., 2011. Leptin regulates the reward value of nutrient. Nat. Neurosci. 14, 1562–1568. http://dx.doi.org/10.1038/nn.2977.

Ferenczi, E.A., Zalocusky, K.A., Liston, C., Grosenick, L., Warden, M.R., Amatya, D., Katovich, K., Mehta, H., Patenaude, B., Ramakrishnan, C., Kalanithi, P., Etkin, A., Knutson, B., Glover, G.H., Deisseroth, K., 2016. Prefrontal cortical regulation of brainwide circuit dynamics and reward-related behavior. Science 351. http://dx.doi.org/10.1126/science.aac9698.

Gozzi, A., Jain, A., Giovanelli, A., Bertollini, C., Crestan, V., Schwarz, A.J., Tsetsenis, T., Ragozzino, D., Gross, C.T., Bifone, A., 2010. A neural switch for active and passive fear. Neuron 67, 656–666. http://dx.doi.org/10.1016/j.neuron.2010.07.008.

Groenewegen, H.J., 1988. Organization of the afferent connections of the mediodorsal thalamic nucleus in the rat, related to the mediodorsal prefrontal topography. Neuroscience 24, 379–431.

Groenewegen, H.J., Berendse, H.W., Haber, S.N., 1993. Organization of the output of the ventral striatopallidal system in the rat: ventral pallidal efferents. Neuroscience 57, 113–142. http://dx.doi.org/10.1016/0306-4522(93)90115-V.

Honey, G., Bullmore, E., 2004. Human pharmacological MRI. Trends Pharmacol. Sci. 25, 366–374. http://dx.doi.org/10.1016/j.tips.2004.05.009.

Humphries, M.D., Prescott, T.J., 2010. The ventral basal ganglia, a selection mechanism at the crossroads of space, strategy, and reward. Prog. Neurobiol. 90, 385–417. http://dx.doi.org/10.1016/j.pneurobio.2009.11.003.

Ikemoto, S., 2007. Dopamine reward circuitry: two projection systems from the ventral midbrain to the nucleus accumbens-olfactory tubercle complex. Brain Res. Rev. 56, 27–78. http://dx.doi.org/10.1126/scisignal.2001449.Engineering.

Ikemoto, S., 2002. Ventral Striatal Anatomy of Locomotor Activity Induced By Cocaine, D -Amphetamine, Dopamine and D1/D2 Agonists 1 113, 939–955.

Jenkins, B.G., 2012. Pharmacologic magnetic resonance imaging (phMRI): imaging drug action in the brain. Neuroimage 62, 1072–1085. http://dx.doi.org/10.1016/j.neuroimage.2012.03.075.

Kenny, P.J., Voren, G., Johnson, P.M., 2013. Dopamine D2 receptors and striatopallidal transmission in addiction and obesity. Curr. Opin. Neurobiol. 23, 1–4. http://dx.doi.org/10.1016/j.conb.2013.04.012.

Kupchik, Y.M., Brown, R.M., Heinsbroek, J.A., Lobo, M.K., Schwartz, D.J., Kalivas, P.W., 2015. Coding the direct/indirect pathways by D1 and D2 receptors is not valid for accumbens projections. Nat. Neurosci. 18, 1230–1232. http://dx.doi.org/10.1038/nn.4068.

Lee, H.J., Weitz, A.J., Bernal-casas, D., Kravitz, A.V., Kreitzer, A.C., Lee, H.J., Weitz, A.J., Bernal-casas, D., Duffy, B.A., Choy, M., Kravitz, A.V., 2016. Activation of direct and indirect pathway medium spiny neurons drives distinct brain-wide responses. Neuron 91, 1–13. http://dx.doi.org/10.1016/j.neuron.2016.06.010.

Lee, J.H., Durand, R., Gradinaru, V., Zhang, F., Goshen, I., Kim, D.-S., Fenno, L.E., Ramakrishnan, C., Deisseroth, K., 2010a. Global and local fMRI signals driven by neurons defined optogenetically by type and wiring. Nature 465, 788–792. http://dx.doi.org/10.1038/nature09108.

Lee, J.H., Durand, R., Gradinaru, V., Zhang, F., Goshen, I., Kim, D.-S., Fenno, L.E., Ramakrishnan, C., Deisseroth, K., 2010b. Global and local fMRI signals driven by neurons defined optogenetically by type and wiring. Nature 465, 788–792. http://dx.doi.org/10.1038/nature09108.

Leslie, R.A., James, M.F., 2000. Pharmacological magnetic resonance imaging: a new application for functional MRI. Trends Pharmacol. Sci. 21, 314–318.

Lohani, S., Poplawsky, A.J., Kim, S.-G., Moghaddam, B., 2016. Unexpected global impact of VTA dopamine neuron activation as measured by opto-fMRI. Mol. Psychiatry 0, 1–10. http://dx.doi.org/10.1038/mp.2016.102.

Malik, S., McGlone, F., Bedrossian, D., Dagher, A., 2008. Ghrelin modulates brain activity in areas that control appetitive behavior. Cell Metab. 7, 400–409. http://dx.doi.org/10.1016/j.cmet.2008.03.007.

Mandeville, J.B., Liu, C.H., Vanduffel, W., Marota, J.J.A., Jenkins, B.G., 2014. Data collection and analysis strategies for phMRI. Neuropharmacology 84, 65–78. http://dx.doi.org/10.1016/j.neuropharm.2014.02.018.

Meredith, G.E., Baldo, B.A., Andrezjewski, M.E., Kelley, A.E., 2008. The structural basis for mapping behavior onto the ventral striatum and its subdivisions. Brain Struct. Funct. 213, 17–27. http://dx.doi.org/10.1007/s00429-008-0175-3.

Paxinos, G., Watson, C., 2005. The Rat Brain in Stereotaxic Coordinates 5th edit. ed.. Academic Press, New York.

Richard, J.M., Berridge, K.C., 2012. Nucleus accumbens dopamine/glutamate interaction switches mode to generate desire versus dread: d1 alone for appetitive eating but D1 and D2 together for fear. J. Neurosci. 31, 12866–12879. http://dx.doi.org/10.1523/JNEUROSCI.1339-11.2011.Nucleus.

Rogers, R.D., 2011. The roles of dopamine and serotonin in decision making: evidence from pharmacological experiments in humans. Neuropsychopharmacology 36, 114–132. http://dx.doi.org/10.1038/npp.2010.165.

Russo, S.J., Nestler, E.J., 2013. The brain reward circuitry in mood disorders. Nat. Rev. Neurosci. 14, 609–625. http://dx.doi.org/10.1038/nrn3381.

Salamone, J.D., Correa, M., 2012. The mysterious motivational functions of mesolimbic dopamine. Neuron 76, 470–485. http://dx.doi.org/10.1016/j.neuron.2012.10.021.

Schmid, F., Wachsmuth, L., Albers, F., Schwalm, M., Stroh, A., Faber, C., 2016. True and apparent optogenetic BOLD fMRI signals. Magn. Reson. Med. 0, 1–11. http://

dx.doi.org/10.1002/mrm.26095.
Schultz, W., 2013. Updating dopamine reward signals. Curr. Opin. Neurobiol. 23, 229–238. http://dx.doi.org/10.1016/j.conb.2012.11.012.
Urban, D.J., Roth, B.L., 2015. DREADDs (Designer Receptors Exclusively Activated by Designer Drugs): chemogenetic tools with therapeutic utility. Annu. Rev. Pharmacol. Toxicol. 55, 399–417. http://dx.doi.org/10.1146/annurev-pharmtox-010814-124803.
van Zessen, R., van der Plasse, G., Adan, R.A.H., 2012. Contribution of the mesolimbic dopamine system in mediating the effects of leptin and ghrelin on feeding. Proc. Nutr. Soc. 71, 435–445. http://dx.doi.org/10.1017/S0029665112000614.
Verma, S.P., Quiroz-Ruiz, A., 2006. Critical values for 22 discordancy test variants for outliers in normal samples up to sizes 100, and applications in science and engineering. Rev. Mex. Cienc. Geol. 23, 302–319.
Voss, H.U., Ballon, D.J., Domingos, A.I., 2011. Neuronal and hemodynamic source modeling of optogenetic BOLD signals. 2011 IEEE Signal Process. Med. Biol. Symp. 1–6. ⟨http://dx.doi.org/10.1109/SPMB.2011.6120104⟩.
Wang, G.J., Smith, L., Volkow, N.D., Telang, F., Logan, J., Tomasi, D., Wong, C.T., Hoffman, W., Jayne, M., Alia-Klein, N., Thanos, P., Fowler, J.S., 2012. Decreased dopamine activity predicts relapse in methamphetamine abusers. Mol. Psychiatry 17, 918–925. http://dx.doi.org/10.1038/mp.2011.86.
Wise, R.A., 2004. Dopamine, learning and motivation. Nat. Rev. Neurosci. 5, 483–494. http://dx.doi.org/10.1038/nrn1406.